Supporting information

Anchoring of Black Phosphorus Quantum Dots onto WO_3 Nanowires to Boost Photocatalytic CO_2 Conversion into Solar Fuels

Wa Gao,[a,†] Xiaowan Bai,[c,†] Yuying Gao,[e,f,†] Jinqiu Liu,[a] Huichao He,[b] Yong Yang,[d] Qiutong Han,[a] Xiaoyong Wang,[a] Xinglong Wu,[a] Jinlan Wang,[c,] Fengtao Fan,[e,*] Yong Zhou,[a,*] Can Li,[e] Zhigang Zou[a]*

National Laboratory of Solid State Microstructures, Collaborative Innovation Center of Advanced Microstructures, Jiangsu Key Laboratory for Nano Technology, School of Physics, Nanjing University, Nanjing 210093, P. R. China. E-mail: zhouyong1999@nju.edu.cn.

[b] State Key Laboratory of Environmental Friendly Energy Materials, School of Materials Science and Engineering, Southwest University of Science and Technology, Mianyang, Sichuan 621010, P. R. China.

[c] School of Physics, Southeast University, Nanjing 211189, P. R. China. Email: jlwang@seu.edu.cn.

[d] Key Laboratory of Soft Chemistry and Functional Materials (MOE), Nanjing University of Science and Technology, Nanjing 210094, P. R. China.

[e] State Key Laboratory of Catalysis, iChEM, Dalian Institute of Chemical Physics, CAS, Dalian National Laboratory for Clean Energy, Dalian 116023, P. R. China. E-mail: ftfan@dicp.ac.cn.

[f] University of Chinese Academy of Sciences, 19A Yuquan Road, Beijing 100049, P. R. China.

† W. Gao, X. Bai, and Y. Gao contributed to this work equally.

Experimental section

Materials:

Sodium tungstate dihydrate (Aladdin, 99.5%) was used as a precursor for the preparation of WO_3. BP (> 99.998 %, Nanjing XFNANO Materials TECH Co., Ltd, P.R. China) was used as a precursor for the preparation of BPQDs. Ammonium acetate was the product of Aladdin, and other chemicals used in the experiments were purchased from the Shanghai Chemical Reagent Company.

Synthesis of BPQD-WO_3 heterostructure:

Ultrasmall BPQDs were immbolized onto the ultrathin WO_3 nanowire by hydrothermal approach. Three steps were taken to prepare the sample, illustrated in the Figure S1. BPQDs were prepared by sonication-assisted liquid exfoliation processes from commercial BP crystalline powders. WO_3 nanowire were synthesized by hydrothermal approach. Afterwards, WO_3 nanowire was added into the homogeneous BPQDs solution. The solution was transferred to a Teflon-lined stainless steel autoclave. The autoclave was sealed and heated. After naturally cooling to room temperature, the solid products were subjected to centrifugation, washed with distilled water and ethanol three times, and finally dried by lyophilization. As for changing the relative concentration between BPQDs and WO_3, we choose one cuvette of BPQDs and WO_3, divided equally into several parts, respectively. It is noted that the concentrations of the three BP solutions were controlled as about 0.489 mg mL^{-1}, as determined by inductive coupled plasma with atomic emission spectroscopy (ICP-AES). Samples with the different mass ratio of about 1%, 3%, 7%, and 10% of the BPQDs to WO_3 were investigated, named as BW-1, BW-2, BW-3, and BW-4, respectively.

Characterization:

The crystal structures were characterized using a Brucker-D8-Advanced X-ray diffraction equipped with Cu Ka radiation source. The FT-IR spectra were measured

by a Nicolet NEXUS870 (USA) spectrometer. Raman spectra were acquired on a T6400 triple micro-Raman system using the 514.5 nm line of an Ar^+ laser as the excitation source. Morphologies of the samples were observed by field-emission scanning electron microscopy (FESEM, HITACHI S-4800) equipped with an energy-dispersive X-ray spectroscopy (EDS, Oxford instruments X-Max). Transmission electron microscopy (TEM) images were recorded by an FEI Tecnai F20 microscope at an accelerating voltage of 100 kV. X-ray photoelectron spectroscopy (XPS) was carried out on an RBD upgraded PHI-5000C ESCA system (Perkin-Elmer) with Mg Kα radiation (hυ = 1253.6 eV). The binding energy of C1s (284.6 eV) was used to calibrate the other binding energies. UV-vis diffuse reflectance spectroscopy (UV-vis-DRS) was measured on a Shimadzu UV-2600 spectrometer. Photoluminescence (PL) emission spectra were recorded on a PerkinElmer LS 55 Fluorescence spectrometer at 355 nm. The fluorescence emission decay time data were obtained on a Horiba Jobin-Yvon Fluorolog-3-21-TCSPC spectrometer.

Photocatalytic Experiments:

For the photocatalytic reduction of CO_2, 10 mg of sample was uniformly dispersed on the glass reactor with an area of 4.2 cm^2. A 300 W Xenon arc lamp was used as the light source of photocatalytic reaction. The volume of reaction system was about 460 ml. Before the irradiation, the system was vacuum-treated several times, and then the high purity of CO_2 gas was followed into the reaction setup for reaching ambient pressure. 0.4 mL of deionized water was injected into the reaction system as reducer. The as-prepared photocatalysts were allowed to equilibrate in the CO_2/H_2O atmosphere for several hours to ensure that the adsorption of gas molecules was complete. During the irradiation, about 1 mL of gas was continually taken from the reaction cell at given time intervals for subsequent CO concentration analysis by using a gas chromatograph (GC-2014C, Shimadzu Corp., Japan).

SPV measurement:

Photo-irradiated KPFM (Bruker Dimension Icon SPM system) technique performs surface topography and surface potential measurements in the amplitude-modulated (AM) mode by exciting the cantilever electrically and mechanically at the same time. under an ambient atmosphere.The Pt/Ir coated condutive probe (resonant frequency 72 kHz) was used. The surface potential is the surface work function difference between tip and sample. Images were acquired at scan rates of 0.5 Hz, and tip lift height was set to 20 nm at tapping mode for surface potential mapping. The surface photovoltage (SPV) mappings were obtained from the difference in surface potential of samples in the dark and under illumination. The SPV was directly related to the photogenerated charge separation, whose amplitude and signal denoted the ability of the charge separation and the direction of charge transport, respectively. Monochromatic light was obtained from the light of a 300 W xenon arc lamp (PLS-SXE300 (Beijing Perfectlight Co. Ltd)) using a Zolix Omni- λ 500 monochromator and was focused on the sample using a lens with inclined angle of 4°. For KPFM measurement, the samples were spin-coated onto highly doped silicon wafers (n+, 0.05 Ω cm).

Computational details:

All calculations were performed with the Vienna ab initio simulation package (VASP 5.4.1). The Perdew-Burke-Ernzerhof (PBE) functional within the generalized gradient approximation (GGA) was used to describe the exchange correlation energy. Electron-nucleus interaction was treated with the projector augmented wave (PAW) method. The cutoff energy of 450 eV was adopted. The convergence threshold was set as 10^{-4} eV for total energy and 0.02 eV/Å for atomic forces, respectively. To evaluate the effect of van der Waals (vdW) interactions, the semiempirical correction scheme of Grimme (DFT-D2). calculations were performed for armchair (AC) and zigzag (ZZ) edges of black phosphorus (BP). The K-points were set to be 3×1×1 for the AC edge and 1×3×1 for the ZZ edge. The vacuum layers were larger than 15 Å above all the planes to avoid the unphysical interaction between periodic images.

The computational hydrogen electrode model was used to calculate the Gibbs free energy change (ΔG) in involving ($H^+ + e^-$) pair transfer step, as proposed by Nørskov et al., defined as $\Delta G_n(U) = \Delta G_n(U=0) + neU$, where e is the elementary charge of an electron, n is the number of ($H^+ + e^-$) pairs transferred in reaction and U is the electrode potential versus the reversible hydrogen electrode (RHE). At U=0 V, $\Delta G = \Delta E + \Delta E_{ZPE} - T\Delta S + \int C_P dT + \Delta G_{pH}$, where ΔE is the electronic energy difference directly obtained from DFT calculations, ΔE_{ZPE}, $T\Delta S$ and $\int Cp dT$ are zero-point energy correction, entropy correction and enthalpic temperature correction at T=298.15 K respectively, which were calculated from the vibrational frequencies. The contribution to the free energy for each adsorbate involved in CO reduction to C_2H_4 process was listed in Table S1. ΔG_{pH} is the free energy correction with respect to pH, which can be determined using the following equation: $\Delta G_{pH} = 2.303 \times k_B T \times pH$, where k_B is the Boltzmann constant and the value of pH is assumed to be zero. The onset potential (U_{Onset}) of the whole reduction process is determined by the potential-limiting step which has the most positive ΔG (ΔG_{max}) as computed by: $U_{Onset} = -\Delta G_{max}/e$.

Table S1. Calculated the zero-point energy, entropy, and enthalpic temperature correction of different adsorption species in CO reduction to C_2H_4 process on armchair (AC) and zigzag (ZZ) edges of black phosphorus, respectively. All values are given in eV.

Adsorption Species	AC edge			Adsorption Species	ZZ edge		
	E_{ZPE}	$-TS$	$\int C_P dT$		E_{ZPE}	$-TS$	$\int C_P dT$
*CO-CO	0.44	-0.22	0.11	*CO-CO	0.44	-0.20	0.11
*CO-COH	0.77	-0.22	0.12	*CO-COH	0.75	-0.21	0.11
*CO-CHOH	1.04	-0.26	0.13	*CO-CHOH	1.05	-0.23	0.13
*CO-CH_2OH	1.36	-0.30	0.15	*CO-CH_2+H_2O	1.37	-0.31	0.15
*OCH-CH_2OH	1.69	-0.25	0.13	*OCH-CH_2	0.93	-0.16	0.09

*OCH-CH_2+H_2O	1.23	-0.26	0.12	*OCH-CH_2	1.23	-0.26	0.12
*OCH_2-CH_2	1.58	-0.20	0.10	*OCH_2-CH_2	1.59	-0.15	0.09
*OH	0.36	-0.11	0.06	*OH	0.36	-0.10	0.05

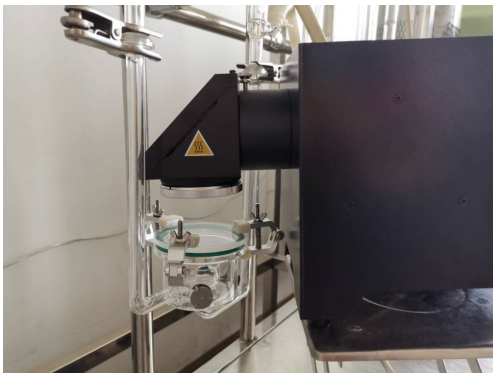

Figure S1. Photographic picture of photocatalytic reactionconversion rate of CO_2.

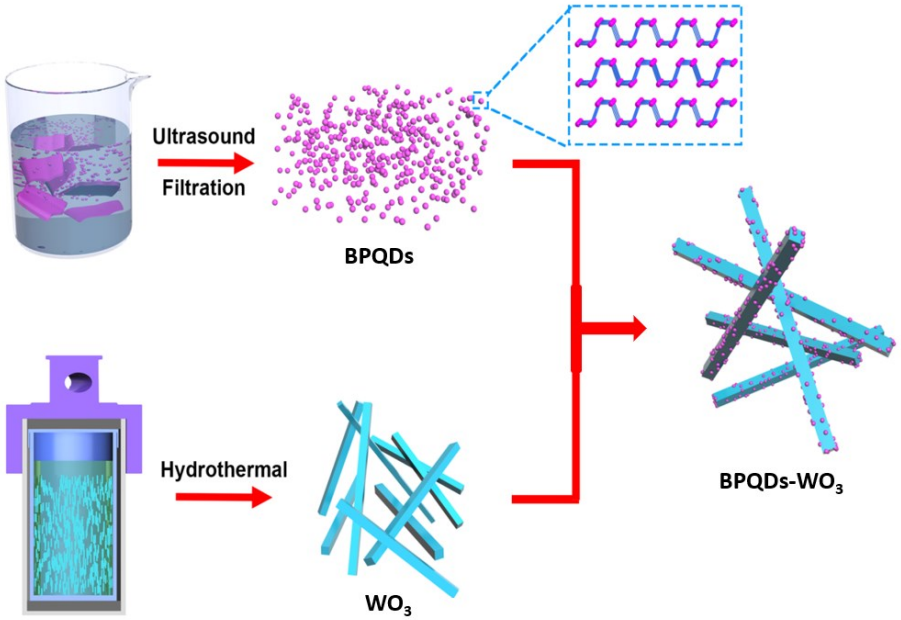

Figure S2. Schematic illustration of the fabrication process of BPQDs-WO_3 hybrids.

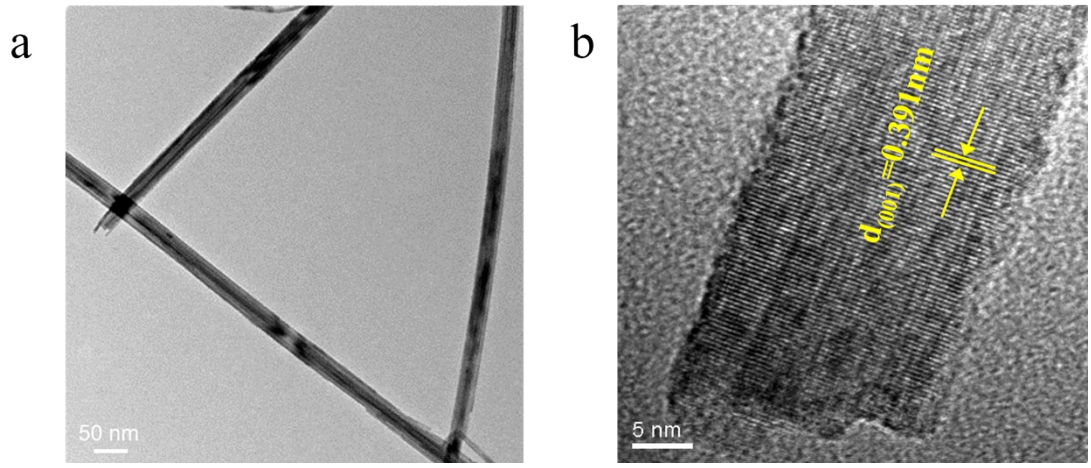

Figure S3. (a) TEM and (b) HRTEM images of WO_3 nanowires.

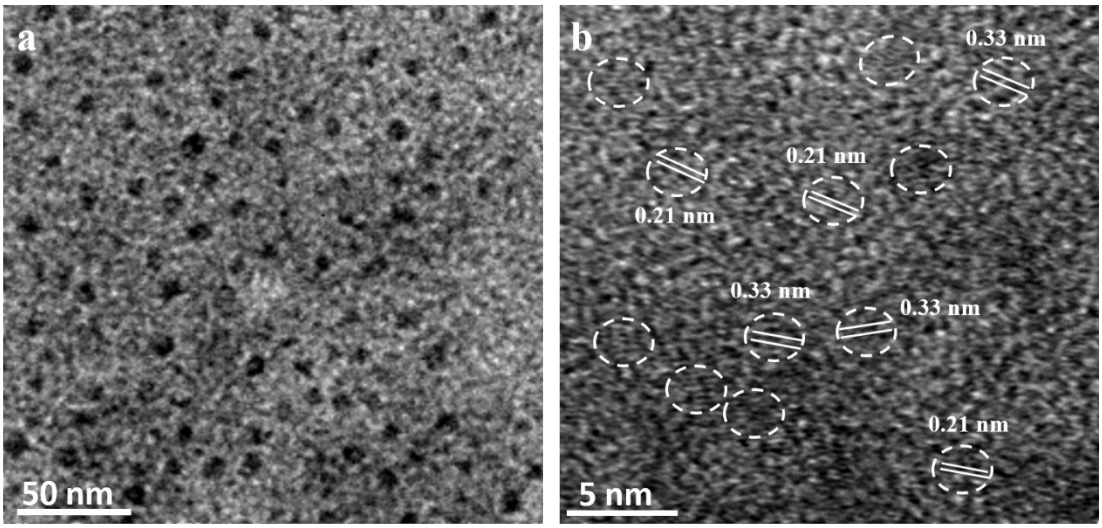

Figure S4. (a) TEM and (b) HRTEM images of BPQDs.

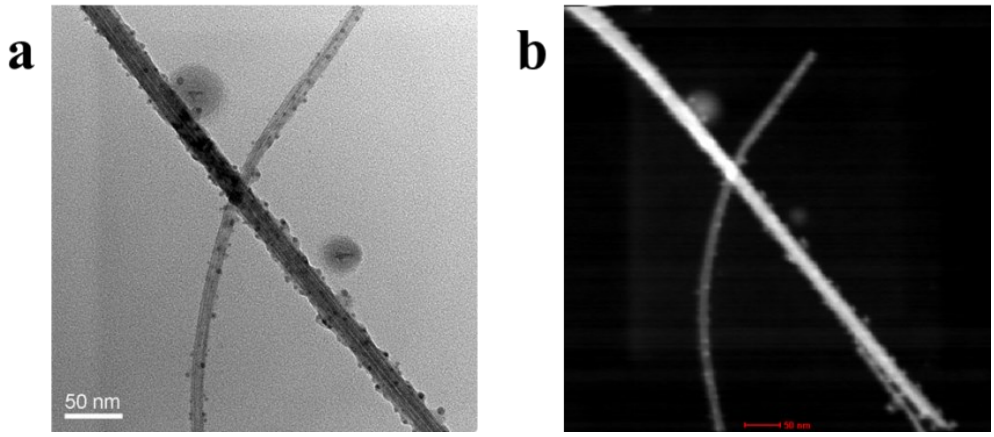

Figure S5. TEM and the corresponding HAADF-STEM images of BW-3.

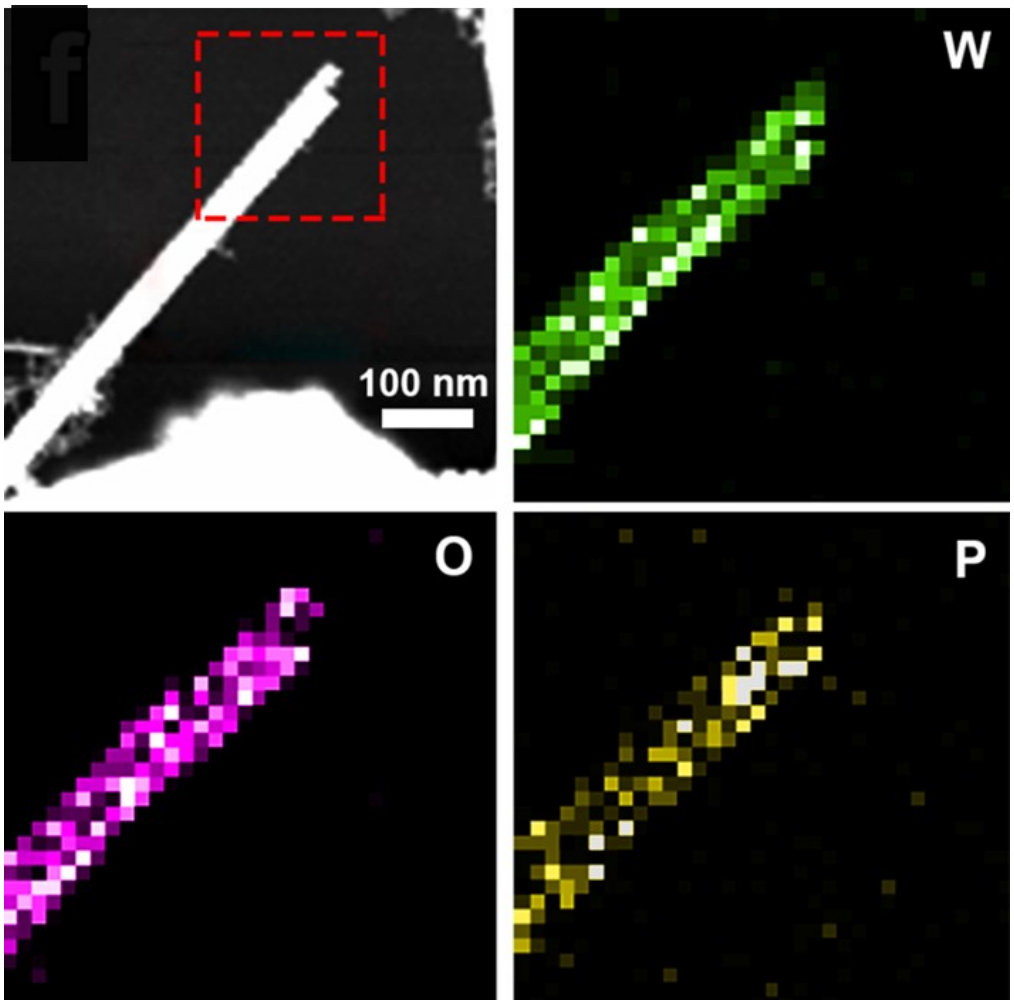

Figure S6. EDX elemental mapping of W, O, and P of BW-3.

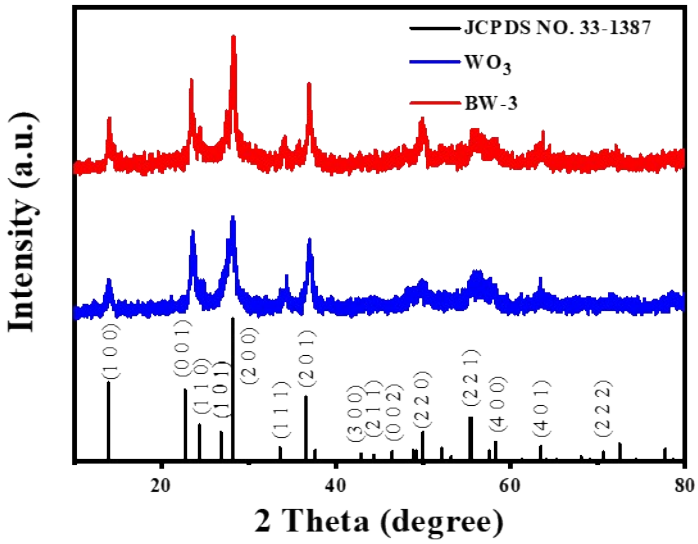

Figure S7. XRD patterns of WO_3 nanowire and BW-3.

The XRD pattern (Figures S6) of the BW-3 show that all the diffraction peaks are readily indexed to the hexagonal phase of WO_3 (JCPDS 33−1387). [12] No observation of the diffraction peaks of the BPQD is possibly due to the low content.

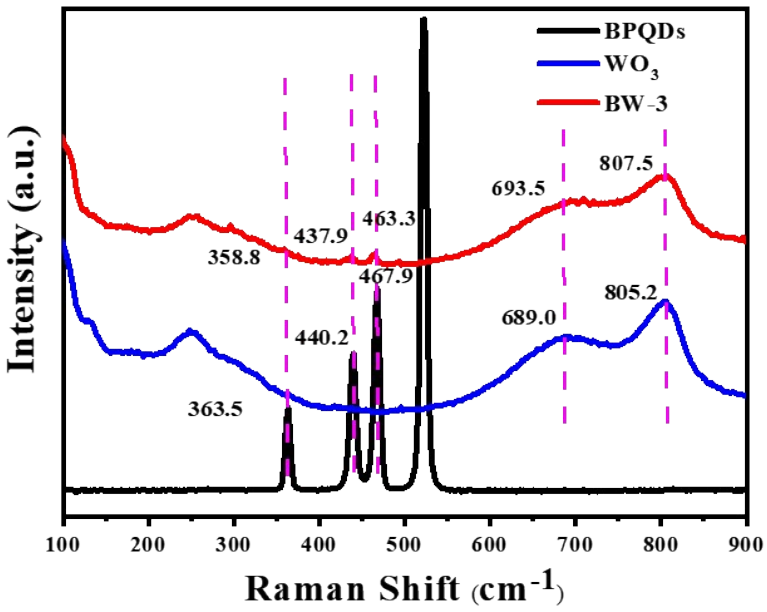

Figure S8. Raman spectra of BPQDs, WO_3 nanowire, and BW-3.

The Raman spectra (Figures S7) of BPQDs, WO_3 nanowire, and BW-3 reveal that the WO_3 nanowire shows vibrational signals in the range of 600–1000 cm^{-1} upon 520 nm light excitation.[15,16] The A_{1g}, B_{2g}, and A_{2g} modes peaks of the BPQD were detected at 363.5, 440.2, and 467.9 cm^{-1}, respectively.[18] With hybridization of the WO_3 and BPQD, the peaks assigning to δO-W-O and νO-W-O was observed red shift about 4.5 cm^{-1} and 2.3 cm^{-1}, respectively. Meanwhile, the A_{1g}, B_{2g}, and A_{2g} modes of the BPQD also exhibit blue shift about 4.7 cm^{-1}, 2.3 cm^{-1}, and 4.6 cm^{-1}, respectively. It indicates the strong electronic interaction between BPQDs and WO_3 nanowire, possibly originating from the intimate contact.

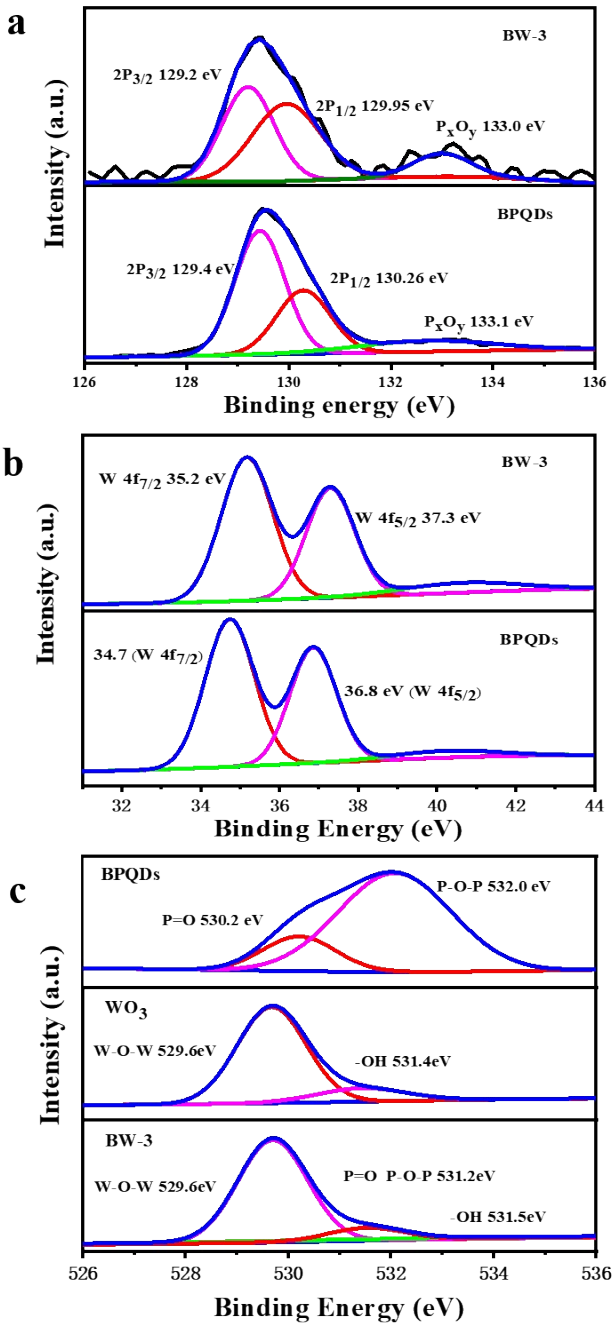

Figure S9. High-resolution XPS core-level spectra of (a) P 2p of BPQDs and BW-3, (b) W 4f of WO_3 and BW-3 and (c) O 1s of BPQDs, WO_3 and BW-3, respectively.

The XPS survey spectra (Figures S8) show that three peaks of the BPQD can be deconvoluted at approximately 129.4, 130.3, and 132.8 eV, corresponding to P $2p_{3/2}$,

P $2p_{1/2}$, and partially oxidized phosphorus (P_xO_y), respectively.[18] Both characteristic peaks assigning to O 2p and W 4f for the WO_3 nanowire were observed, and the latter can be divided into two peaks at 34.7 eV (W $4f_{7/2}$) and 36.8 eV (W $4f_{5/2}$), respectively.[18] With hybridization, the P 2p peaks of the BPQD shifted to the lower binding energies, and the binding energy belonging to W 4f shifted to the higher energies. It further confirms the strong electronic coupling interactions between the WO_3 and BPQD. It is well known that increase of binding energy indicates the weakened electron screening effect due to the decrease of the electron concentration, and the decrease of binding energy means an increase of electron concentration. [5-7] The electron transfer from the WO_3 to BPQDs can be concluded.

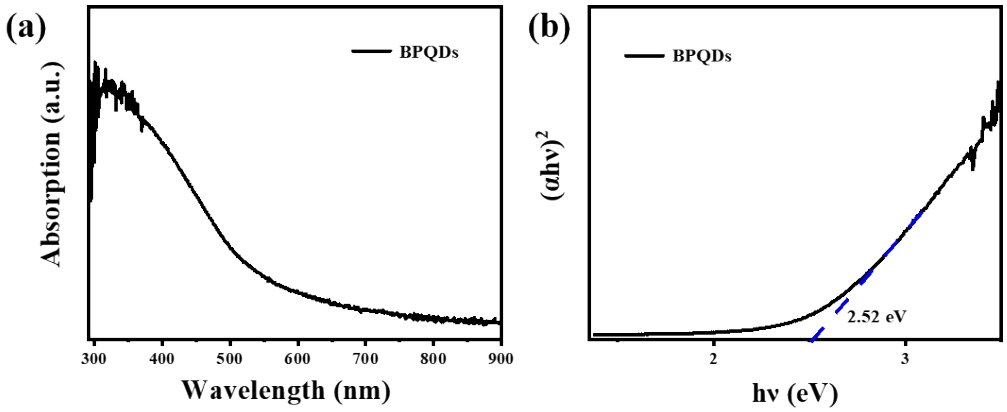

Figure S10. (a) UV-Visible absorption spectra of as-prepared BPQDs. (b) Tauc plot curve of the BPQDs related to the optical bandgap.

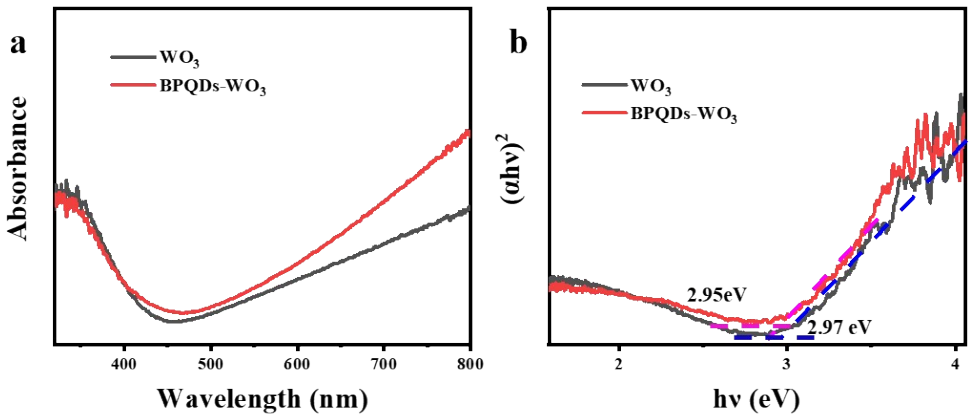

Figure S11. (a) UV-Visible absorption spectra of as-prepared WO_3 and BPQDs-WO_3.

(b) Tauc plot curve of the WO_3 and BPQDs-WO_3 related to the optical bandgap.

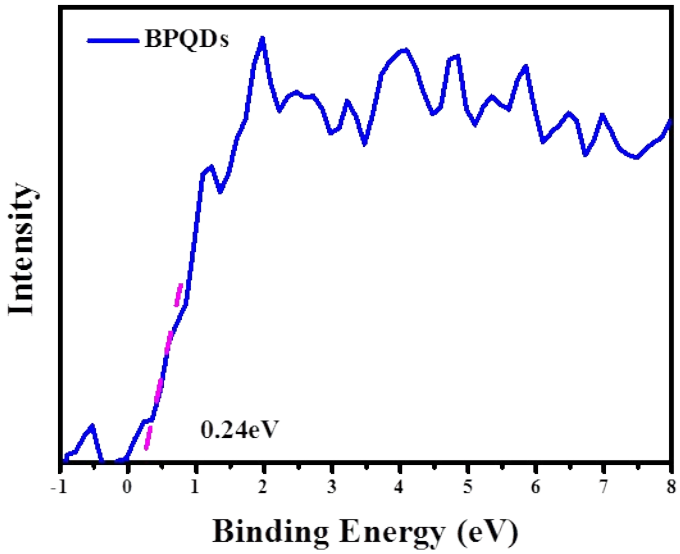

Figure S12. Valence XPS spectra of the BPQDs.

The Vacuum fermi level of BPQDs was estimated to be -5.7 eV. [1] XPS valence band spectrum reveals that the energy level difference between valence band maximum of BPQDs and Fermi level is 0.24 eV. Then, the VB energy (E_{VB}) values of BPQDs was estimated to be -5.94 eV. Combining with the measured Eg from the absorption spectra, the CB energy values (E_{CB}) of BPQDs (3.44 eV) was estimated from $E_{CB} = E_{VB} - E_g$. This value is consistent with the theoretical calculation. These values in eV are all converted to electrochemical energy potentials in V according to the reference standard for which −4.44 eV versus vacuum level equals 0 V versus reversible hydrogen electrode.

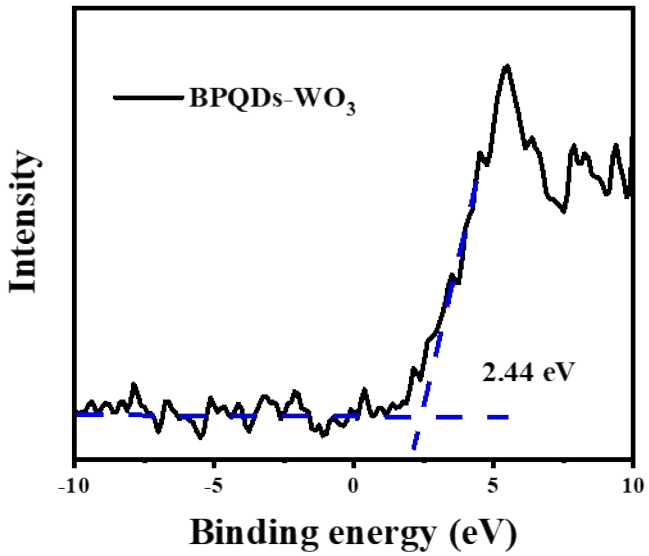

Figure S13. Valence XPS spectra of the BPQDs-WO_3.

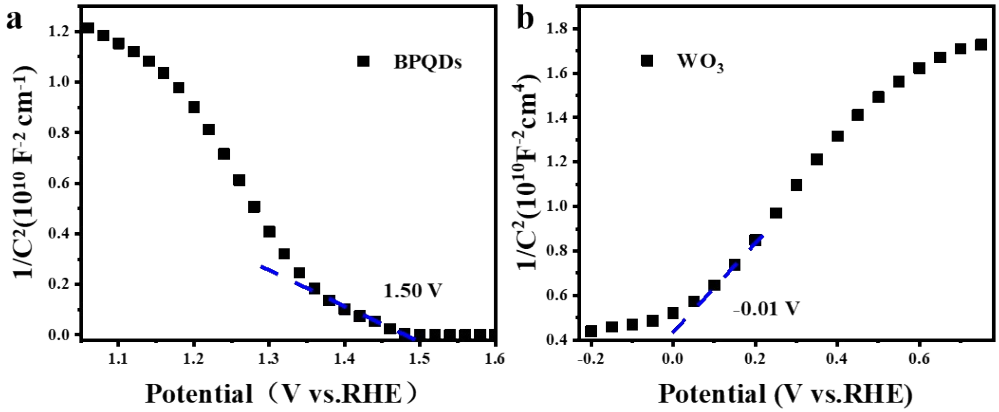

Figure S14. Mott-Schottky of (a) BPQDs and (b) WO_3.

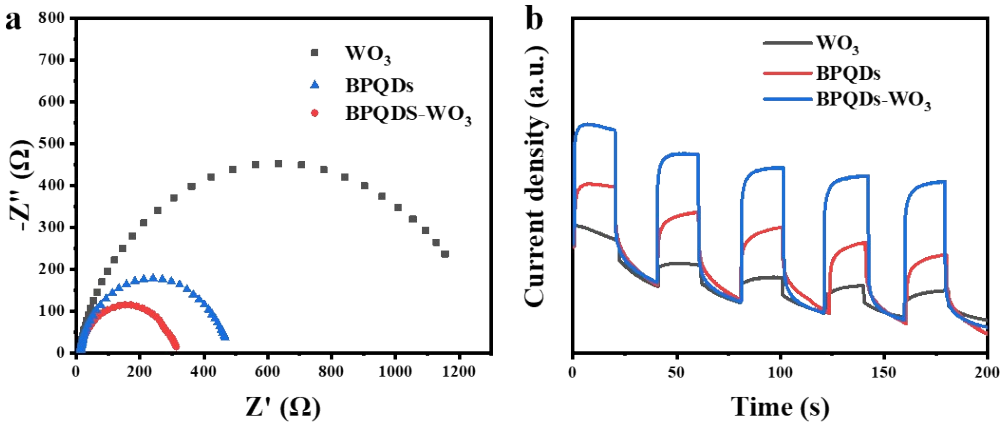

Figure S15. (a) EIS spectra and (b) transient photocurrent spectra of different samples.

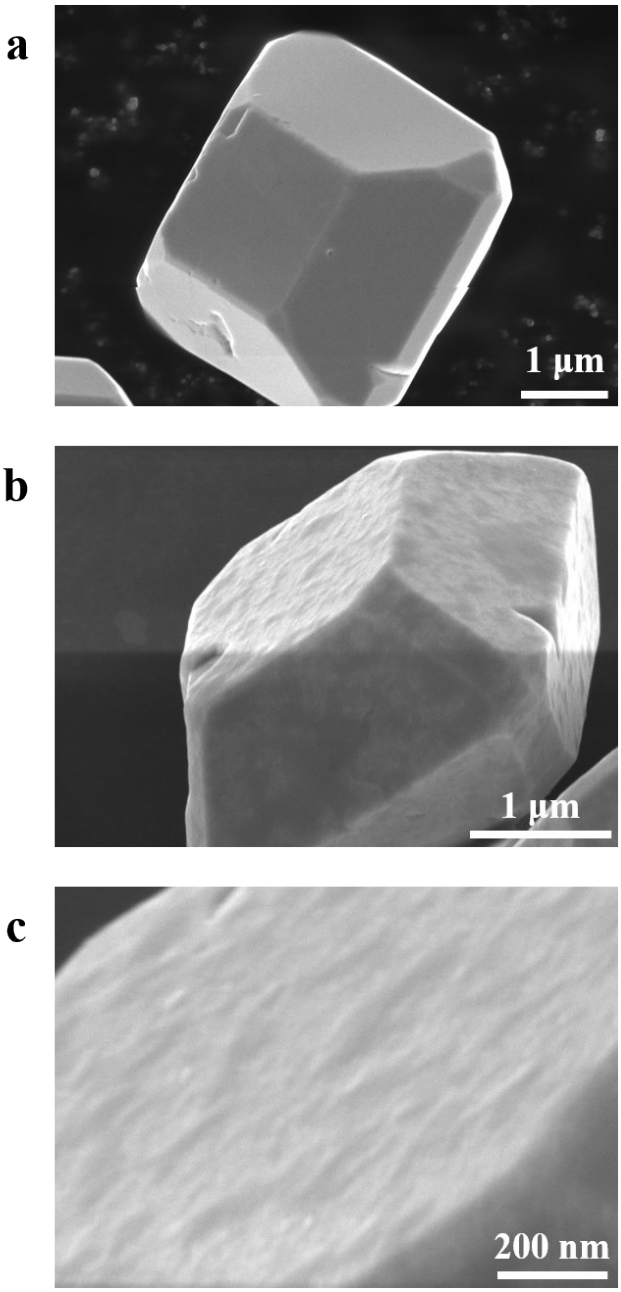

Figure S17. FE-SEM images of (a) applied $BiVO_4$ and (b, c) BPQDs-$BiVO_4$, revealing that the smooth surface of the $BiVO_4$ became relatively rough after coupling BPQDs.

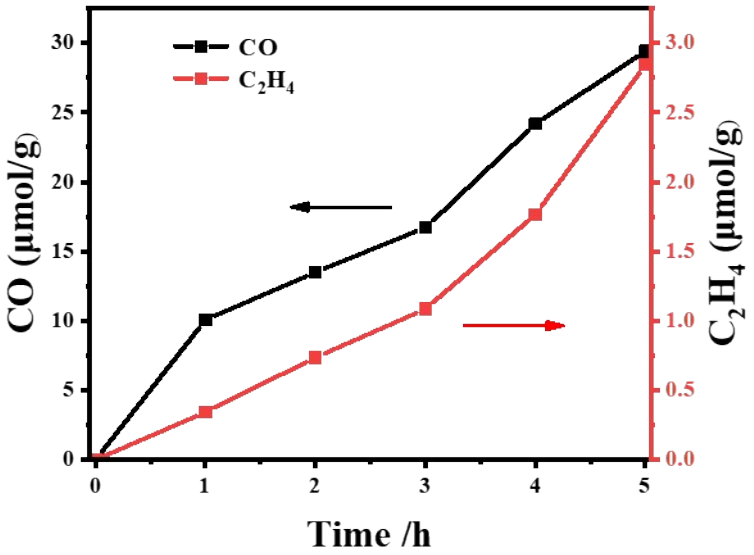

Figure S18. Photocatalytic product evolution amounts for the BPQDs-$BiVO_4$.

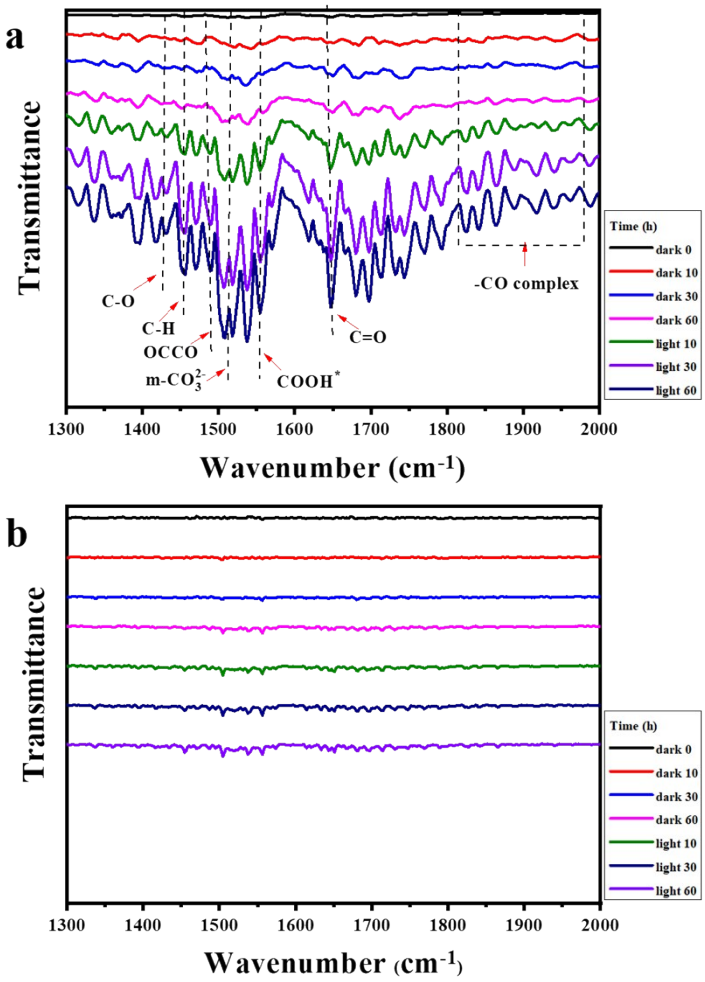

Figure S19. *In situ* FTIR spectra for the adsorption and activation of CO_2 on (a) BW-3 and (b) WO_3.

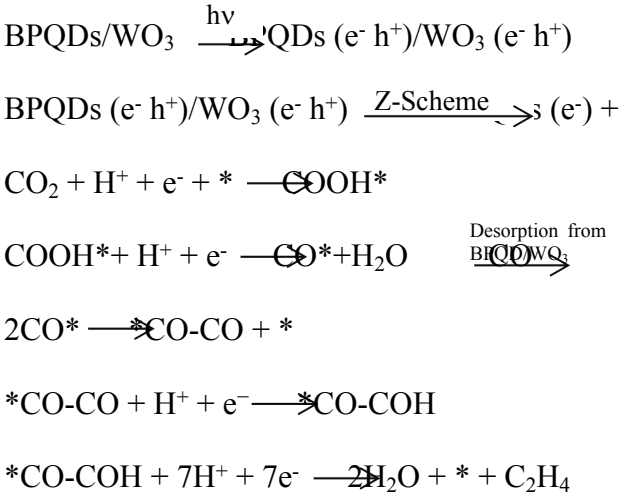

Figure S20. Proposed reaction process for the reduction of CO_2 of the BPQDs-WO_3 hybrids under light illumination. * represents the active reaction site of the catalyst.

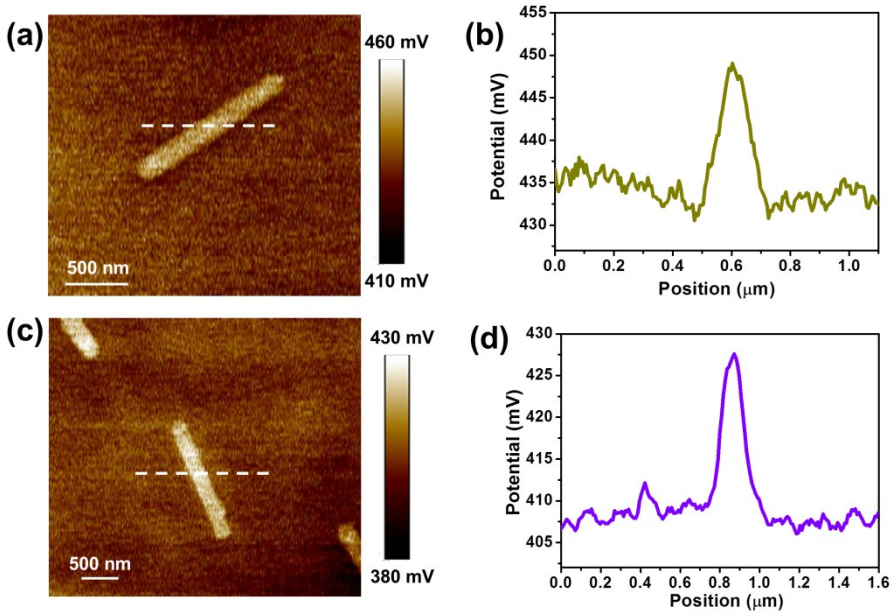

Figure S21. KPFM measurement of WO_3 and BPQD-WO_3. (a, c) Surface potential images of WO_3 (a) and BPQD-WO_3 (c) in the dark. (b, d) Surface potential profiles of WO_3 (b) and BPQD-WO_3 (d) along white lines.

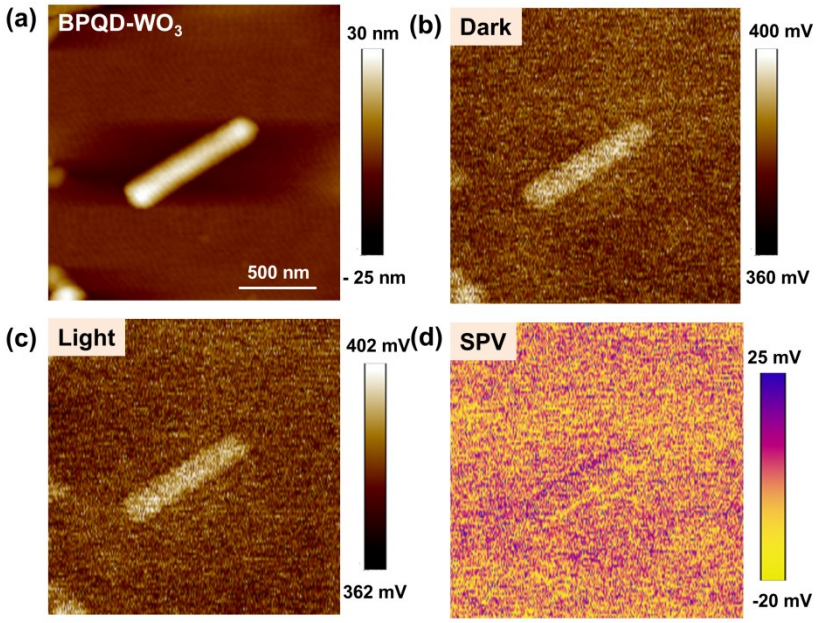

Figure S22. KPFM measurement of BPQD-WO_3. (a) AFM morpholygy of BPQD-WO_3. (b, c) surface potential of BPQD-WO_3 in the dark (b), 620 nm illumination (c). (d) SPV image of BPQD-WO_3.

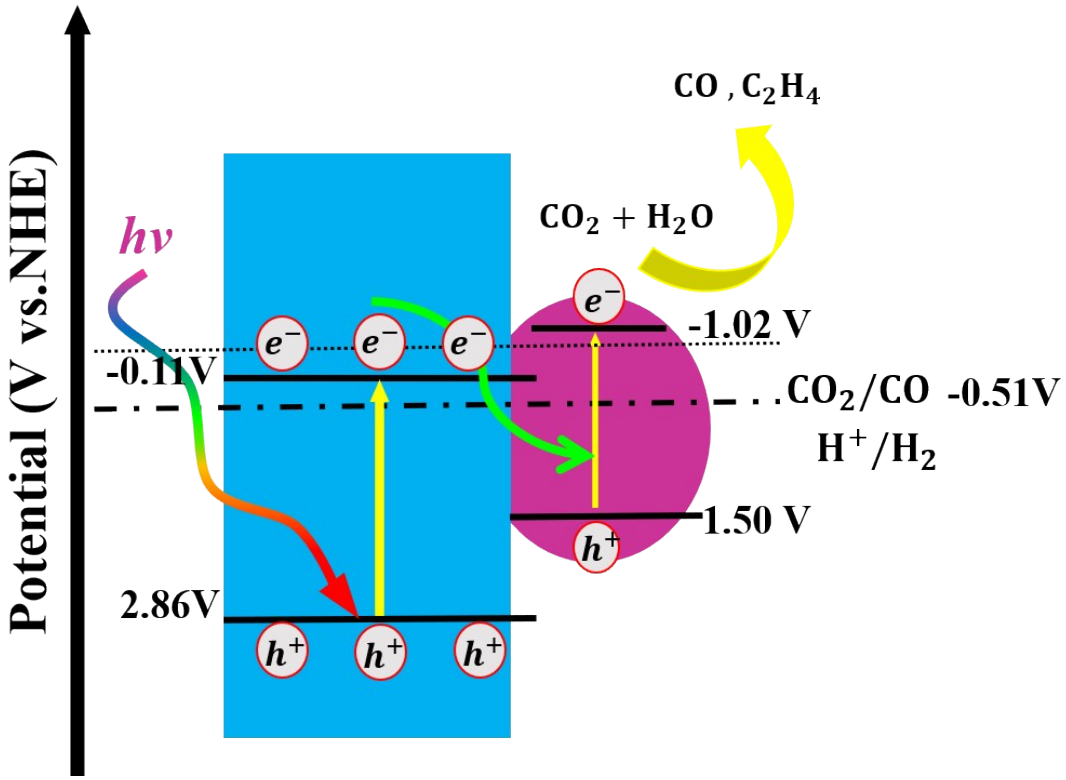

Figure S23. Schematic illustration of Z-scheme photocatalytic CO_2 reduction over the BPQDs-WO_3 nanocomposite under light irradiation.

The flat band potential (quasi Fermi level) is 0.1 V lower than conduction band minimum for n-type semiconductors. As a result, the conduction band minimum of WO_3 is determined −0.11 V. [12]

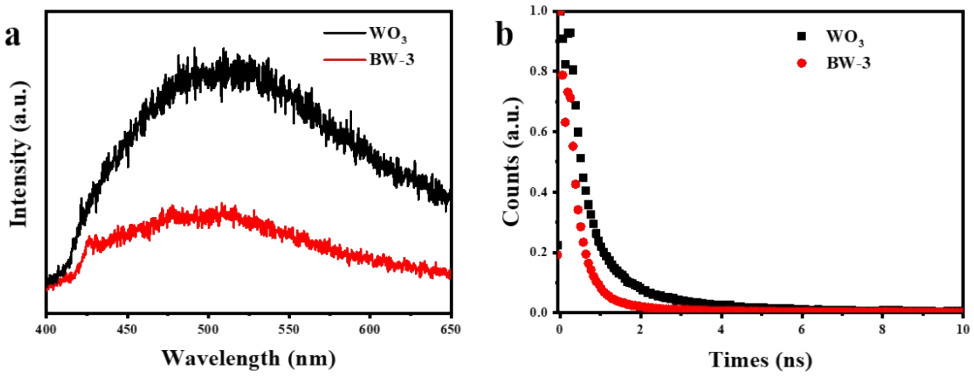

Figure S24. (a) Room-temperature steady-state PL spectra of the WO_3 nanowire and BW-3. (b) Time-resolved PL decay spectra for the WO_3 nanowire and BW-3.